I&EC research
Industrial & Engineering Chemistry Research

Article

Cite This: Ind. Eng. Chem. Res. 2018, 57, 1380−1388

pubs.acs.org/IECR

Quantitative Study on Dissolution Behavior of Nd_2O_3 in Fluoride Melts

Xiaoling Guo,*[,†] Zhi Sun,*[,†,‡] Jilt Sietsma,[†] Bart Blanpain,[§] Muxing Guo,[§] and Yongxiang Yang[†]

[†]Department of Materials Science and Engineering, Delft University of Technology, Mekelweg 2, 2628 CD Delft, The Netherlands

[‡]National Engineering Laboratory for Hydrometallurgical Cleaner Production Technology, Institute of Process Engineering, Chinese Academy of Sciences, 100190 Beijing, China

[§]Department of Materials Engineering, KU Leuven, Kasteelpark Arenberg 44 - Box 2450, 3001 Leuven, Belgium

ABSTRACT: The dissolution of rare earth oxides in molten fluorides is a critical step in the preparation of the corresponding rare earth metals by oxide-fluoride electrolysis. However, quantitatively understanding the nature of dissolution, especially in the case of molten salts, is usually difficult to be achieved by *postmortem* characterization. In this paper, the dissolution behavior of Nd_2O_3 particles in molten fluorides was studied via *in situ* observation with confocal scanning laser microscopy. Combining direct observation with thermodynamic analyses on the oxide dissolution, the rate-limiting step(s) and the effects of parameters like temperature, salt type, and composition on the dissolution rate are identified. This study provides a methodology to estimate the dissolution kinetics of rare earth oxides in molten fluorides during their primary and secondary processing.

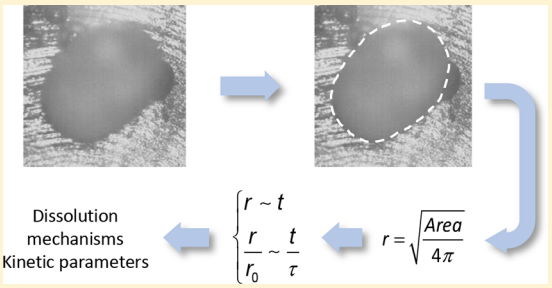

1. INTRODUCTION

As its principal application, over 75% of neodymium is used in the magnet industry.[1] Since their discovery in 1984, NdFeB magnets have been outranking all other materials with respect to magnetic flux density.[2] They have been applied to many advanced technologies, such as miniature high-capacity hard disk drives, compact industrial motors, electric vehicles, and wind turbines.[2] In 2015, the total amount of rare earth metals (REMs) used in NdFeB magnets was around 25 to 30 kt.[3] This accounts for 20% of the total rare earths consumption (calculated based on rare earth oxides).[4] It is estimated that the global demand for rare earth metals in permanent magnets will increase to 40 kt in 2020, which means that annual growth of 7% is foreseen.[3] Therefore, neodymium is categorized in the most critical raw materials, having the highest supply risk in the commission communication on the 2017 List of Critical Raw Materials for the European Union.[5]

Nowadays, oxide-fluoride electrolysis is the dominant technique for the commercial production of neodymium and its alloys from neodymium oxide in both primary and secondary (recycling) production.[6] In the process, neodymium oxide is reduced to metal at the cathode. A mixture of fluorides, mostly containing rare earth fluoride (REF), alkali metal fluoride (AF), and possibly small amounts of alkali earth metal fluorides (AEF), serves as both a solvent for neodymium oxide and an electrolyte for the electrolysis.[7] The electrolysis conditions were found to have significant effects on the process and the current efficiency. One of the critical factors is the feeding rate of neodymium oxide, which needs to be well controlled to ensure smooth production. On the one hand, the deficiency of oxide can lead to the generation of fluorocarbon, covering the graphite anode and inhibiting the electrolysis process. On the other hand, overfeeding can cause a sludge of excess oxide at the bottom of the cell, which is detrimental to the quality of the final products.

A systematic study on the dissolution behavior of Nd_2O_3 in molten fluorides can lead to an improved understanding of its dissolution mechanisms and a quantitative description of the dissolution rate, which would provide crucial theoretical support for feeding control in the industrial production. However, research on the interaction between rare earth oxides and molten salts is almost blank. Stefanidaki et al.[8] and Hu[9] studied the products of the interaction between Nd_2O_3 and fluoride melt with Raman spectroscopy and found the formation of M−O−F (M = metal) complex anions during Nd_2O_3 dissolution. A previous study[10] investigated the interactions of Nd_2O_3 with molten $CaCl_2$ and CaF_2−LiF. It is found that Nd_2O_3 reacted vigorously with $CaCl_2$ to form NdOCl, while Nd_2O_3 gradually dissolved in molten CaF_2−LiF.[10] However, a quantitative discussion of the dissolution process was missing. In the present study, the dissolution of Nd_2O_3 particles in molten fluorides is investigated with confocal scanning laser microscopy (CSLM), which provides *in situ* observation of the dissolution process. This research focuses on understanding the dissolution mechanisms, examining both qualitatively and quantitatively the influencing factors, i.e., temperature, salt type, and composition, and

Received: October 4, 2017
Revised: January 11, 2018
Accepted: January 12, 2018
Published: January 12, 2018

DOI: 10.1021/acs.iecr.7b04125
Ind. Eng. Chem. Res. 2018, 57, 1380−1388

providing a method for predicting the dissolution rate of Nd_2O_3 in LiF-NdF_3.

2. EXPERIMENTAL PROCEDURES

2.1. Materials. The chemicals used in the CSLM experiments are produced by Alfa Aesar with a purity of 99.95 wt %. The compositions of the binary salts, based on LiF, NdF_3, NaF, and KF, are listed in Table 1. Prior to the CSLM experiments, the salts were prepared in a horizontal tube furnace. The chemicals were mixed manually and placed in graphite crucibles before being loaded into the horizontal furnace. The mixtures were heated up to 50 K above their melting points and held for at least 3 h before being quenched with liquid nitrogen. These master salts were crushed into small pieces and kept in a glovebox before the CSLM tests.

Table 1. Composition of the Salts Used in This Study (mol %)

number	LiF	NdF_3	NaF	KF
1	77	23		
2	90	10		
3	95	5		
4		23	77	
5		23		77

The Nd_2O_3 particles were made of pure Nd_2O_3 powder. The powder was isostatically cold pressed into cylinders, which were 2 mm in diameter. The cylinders were then cut into approximately 2 mm in length and sintered at 1773 K for 2 h. The downsizing and rounding of these cylinders were done in an in-house apparatus, in which the air flow was continuously blowing in, and the particles were shaped by continuously hitting the wall of the chamber. The resulting Nd_2O_3 particles were quasi-spherical with a diameter of several hundred micrometers, as shown in Figure 1. Their apparent density at room temperature was measured by the Archimedes' method and determined to be 6.8 ± 0.5 g/cm^3 (the actual density of Nd_2O_3 is 7.24 g/cm^3[11]). Considering that the thermal expansion coefficient of Nd_2O_3 is around 10^{-5}/K,[12] the density of the particle at the experimental temperatures is still higher than that of the melt (about 4.5 g/cm^3 at the experiment temperatures[9]).

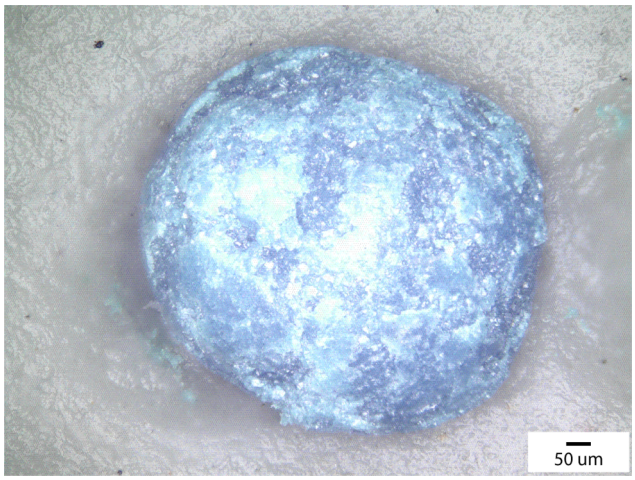

Figure 1. Quasi-spherical Nd_2O_3 particle for dissolution tests.

2.2. Experimental Apparatus and Procedures. The *in situ* observations of the dissolution were conducted with a CSLM-IIF microscope (Lasertec, 1LM21M-SVF17SP). A detailed description of the equipment was given in our previous work.[13] The heating profile was programmed with HiTOS software and controlled by a REX-P300 controller. The heating component is a halogen lamp located at the lower focal point of the elliptical chamber. It can offer a very high heating rate (more than 250 K/min) and cooling rate (more than 500 K/min). A sample holder is placed at the upper focal point of the chamber. The temperature of samples is measured by a B-type thermocouple welded at the bottom of the holder. The experiment temperature was calibrated by measuring the melting points of four standard pure metals, i.e., copper, nickel, palladium, and iron. The actual temperature of the sample was found to be 18 K higher than the measured value in the temperature range of this study. The temperatures indicated in this paper are the actual values.

The CSLM tests were performed under argon (purity >99.99%) atmosphere. The chamber was evacuated and refilled with high purity argon three times to ensure a low oxygen level. Each test began with melting the master salt pieces in a molybdenum crucible. After cooling down, a flat surface was formed. The depth of the melt was about 5 mm, which means that the whole particle can be immersed in the melt during dissolution as its density is higher than the melt, and it should be settled on the bottom of the crucible. The melts used in this study are transparent, which allows easy observation of the particle underneath. Therefore, there is no limitation on the depth of the melt as long as the whole particle can be immersed in it. After melting the master salt in the crucible, a Nd_2O_3 particle was placed on the surface. This started the *in situ* observation of the dissolution process. The observed images were recorded by a camera at a rate of one frame per second for analysis.

Frequently, the particles made in-house were not perfectly spherical as seen in Figure 1. However, the study on particles with irregular shapes that can be approximated to distorted spheres showed that this imperfection would not significantly alter the dissolution curve, and the total dissolution time is the same as the spherical particles with equivalent radii.[14] Therefore, the equivalent radius was applied in postanalysis. It was calculated based on the measured 2D area using an image processing software, ImageJ, with which a border was drawn around the particle, as shown in Figure 2. To minimize the systematic errors in generating the borders, an average radius from three repeats was used in the kinetic study.

Figure 2 is a series of CSLM images taken from the experiments, showing the dissolution of a Nd_2O_3 particle in KF-23NdF_3 at 1141 K. The dashed lines indicate the border of the particle. The shrinkage of the particle can be clearly seen in the images. The equivalent radius of the particle can then be estimated according to the area enclosed by the lines. The left-up corner of the CSLM images shows the time from experiment beginning and the measured temperature. The starting of the dissolution process is when the set temperature is reached. The particle size changing with time can be extracted from 50 to 100 CSLM images with specific time intervals. This relationship will be further analyzed to reveal the dissolution mechanisms and related kinetic parameters.

DOI: 10.1021/acs.iecr.7b04125
Ind. Eng. Chem. Res. 2018, 57, 1380−1388

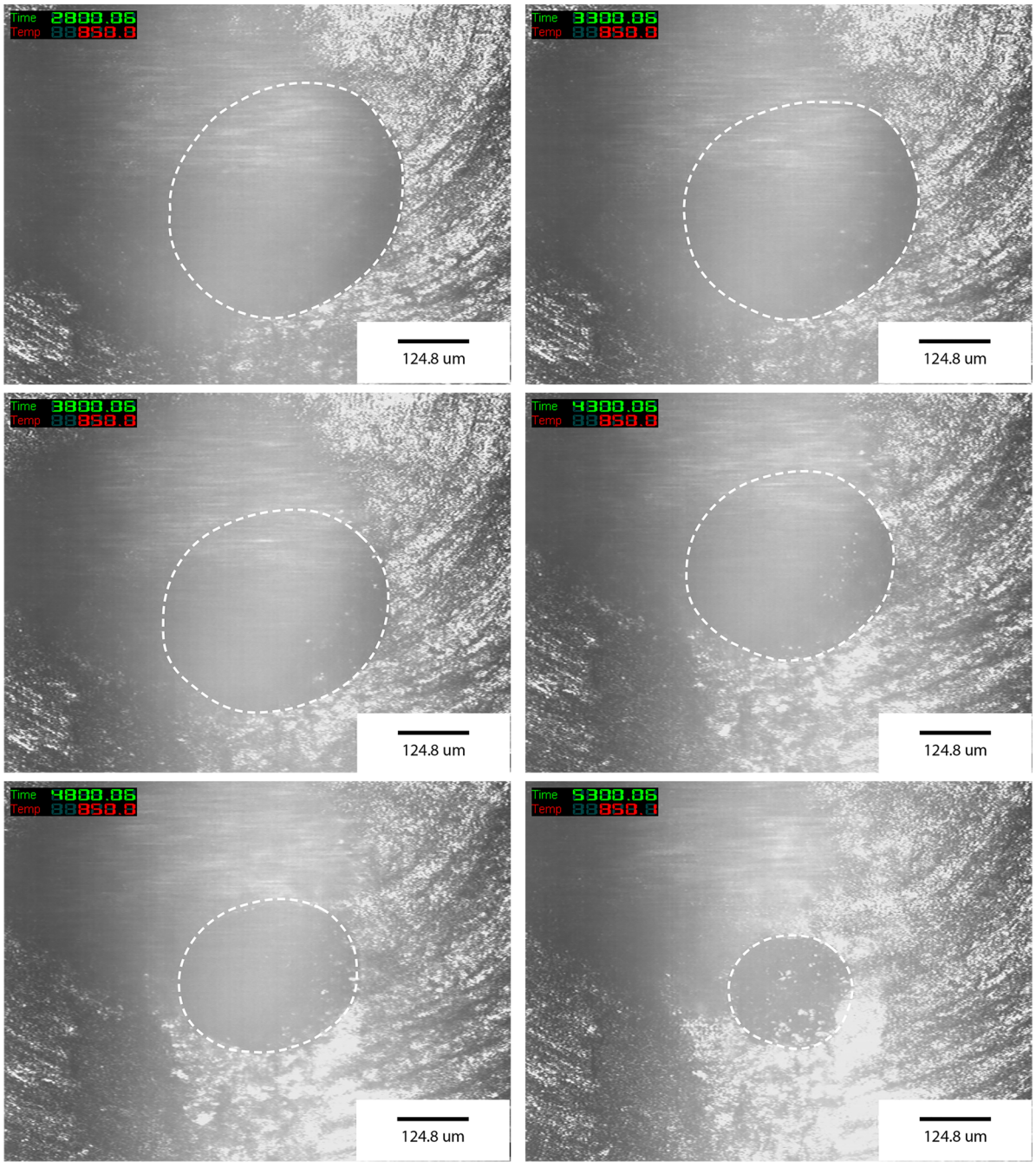

Figure 2. CSLM images of the dissolution of Nd_2O_3 in KF-23NdF_3 at 1141 K.

3. RESULTS AND DISCUSSION

3.1. CSLM *in Situ* Observations. The dissolution of Nd_2O_3 in other melts studied in this paper was very similar to that shown in Figure 2. The dissolution was gradual, and no severe reaction was observed. No solid product was formed outside the particle during dissolution. In some cases, a change of particle shape was noticed, possibly due to differences in dissolution rate at spots with different curvature.[14] Qualitatively, it is evident that the dissolution from convex areas is more efficient than from concave ones, resulting in the spheroidization of particles.[14] Simulation on the shape change of a 4-fold symmetrical precipitate during dissolution confirmed the existence of the spheroidization.[14] With the experimental results published in the same paper, the author also demonstrated that the theory could be extrapolated to three dimensions and irregular shapes.[14] The total dissolution time of a 4-fold symmetrical precipitate is the same as that of a circular one with the same amount of solute.[14] Therefore, the equivalent radius is calculated and applied to determine the dissolution mechanisms and related parameters.

During the dissolution, the generation of bubbles was observed, as indicated in Figure 3. The bubbles probably result from the release of trapped air in the particle. This sometimes triggered the rotation of the particle during the dissolution. To make sure that the experimental conditions are fulfilled with the requirements of the physical model for the kinetic study, the experiments were selected so as to exclude those, in which the movement triggered by the release of bubbles was visually significant. The other reason why the movement is considered

DOI: 10.1021/acs.iecr.7b04125
Ind. Eng. Chem. Res. 2018, 57, 1380−1388

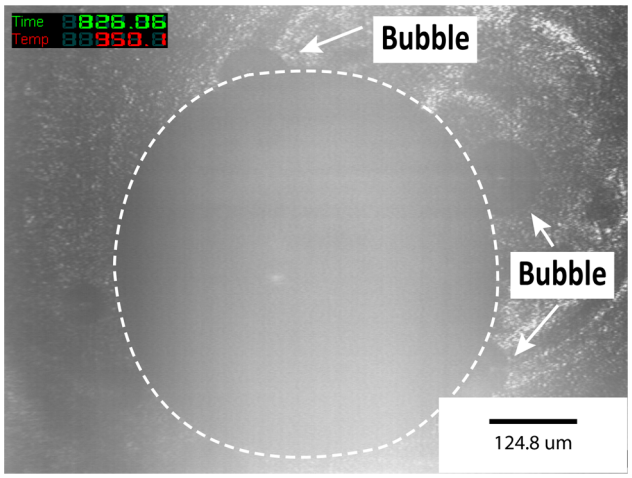

Figure 3. Release of bubbles during the dissolution of Nd_2O_3 particles.

to be insignificant in this research will be discussed in the following section.

3.2. Dissolution Mechanisms. In the literature, the fluid is usually assumed to be stagnant when convection is significantly depressed.[15] In this research, stagnant fluid is assumed because of the following reasons: 1) the particle movement is observed to be minor; 2) the sample size is relatively small to ensure insignificant temperature gradient in the fluid; 3) the heating source with a high power and a low sample amount enables high heating and cooling rates with almost negligible temperature turbulence once a set temperature is reached. Therefore, it is appropriate to assume that the fluid is stagnant as shown in related references for this type of research.[16]

For the dissolution without solid products in a stagnant fluid, the process involves (i) the chemical reaction that transfers atoms or molecules across the phase interface and (ii) the diffusion of solute in the melt.[17] These two steps determine the dissolution rate. In two limiting cases, the process can be reaction-controlled or diffusion-controlled.

Under the assumption of the chemical reaction controlling the dissolution process, the relationship between the radius and dissolution time is obtained as[18]

$$\frac{r}{r_0} = 1 - \frac{t}{\tau} \tag{1}$$

where r and r_0 are the actual and original particle radius in m, respectively, and t and τ are the actual time and total dissolution time in s, respectively. The rate of dissolution (dr/dt) is constant in this case and equal to $-r_0/\tau$.

For diffusion-controlled dissolution that follows Fick's second law, the exact solution for spheres is not available.[19] Approximate solutions are alternatives for solving related problems. To select an appropriate approximation,[20] the supersaturation index k is a crucial physicochemical parameter, expressing the supersaturation ratio, defined as[19]

$$k \equiv \frac{2(C_I - C_M)}{C_P - C_I} \tag{2}$$

where C_M is the far-field concentration of the solute in the solution in mol/L, C_P is the composition of the particle in mol/L, which is taken as a constant in this study, and C_I is the equilibrium concentration of the solute at the interface in mol/L.

C_M equals the original composition of the melt. As the melt did not contain any Nd_2O_3 at the beginning, C_M is zero under the experimental conditions.

C_P represents the density of the solute in the particle. If the particle contains the solute purely, C_P can be calculated directly from the particle density, which is 6.8 g/cm^3 in this study

$$C_P = 6.8\ \text{g/cm}^3 = \frac{6.8\ \text{g/cm}^3 \times 1000\ \text{cm}^3/\text{L}}{M_{Nd_2O_3}\ (\text{g/mol})}$$
$$= \frac{6.8\ \text{g/cm}^3 \times 1000\ \text{cm}^3/\text{L}}{336.5\ \text{g/mol}} = 20\ \text{mol/L} \tag{3}$$

For Nd_2O_3-fluoride systems, the equilibrium concentration can be calculated via

$$C_I = \frac{s_{Nd_2O_3}}{V_m} \tag{4}$$

where $s_{Nd_2O_3}$ is the solubility of Nd_2O_3 in the melt in mol %, and V_m is the molar volume of the specific mixture in L/mol. The Nd_2O_3 solubility in molten fluorides is low (see Table 2),[21] which means that

$$C_I \ll C_P \tag{5}$$

Table 2. Nd_2O_3 Solubility in LiF-23NdF_3

parameter	values			
temperature (K)	868	918	968	1018
solubility (mol %)	0.24	0.28	0.33	0.38

The definition of k can be approximated to

$$k \approx \frac{2C_I}{C_P} \tag{6}$$

The values of k for the systems studied in this paper are listed in Table 3. Due to the lack of solubility data for other binary systems, only the k values for LiF-23NdF_3 are available. It can be seen that the k values in the systems are always small, and the dissolution in such systems is governed by the concentration profile in a steady state, which is the same in one system and determined by C_I, C_M, and C_P.[20] This also suggests that the influence of the transition period before steady state is negligible. When a small disturbance occurs, the influence of the interruption before the establishment of a new stable concentration field is considered to be insignificant. The dissolution would continue as that before the disturbance. Screening the experiments with obvious movement, it is acceptable to hypothesize that the dissolution takes place in a stagnant fluid and the particle position is fixed.

The k values are in the range of 0.018−0.022, in which the invariance-field (IF) approximation is a good choice considering its accuracy to describe a diffusion-controlled process.[20] In the IF approximation, the relationship between particle radius and time is described by[19]

$$\frac{r}{r_0} = \left(1 - \frac{t}{\tau}\right)^{1/2} \tag{7}$$

The theoretical dissolution curves of interface reaction (IR) control (eq 1) and of diffusion control (eq 7) are shown in Figure 4. Comparing the experimental data with theoretical curves can reveal the rate-limiting step(s) of the dissolution.

DOI: 10.1021/acs.iecr.7b04125
Ind. Eng. Chem. Res. 2018, 57, 1380−1388

Table 3. Summary of Experimental Conditions and Related Parameters[d]

melt	T (K)	C_I (mol/L)	C_M (mol/L)	C_P (mol/L)	k	r_0 (μm)	τ (s)	kD (10^{-10}m^2/s)	D (10^{-10}m^2/s)
LiF-23NdF$_3$	1141	0.18[a]	0	20	0.017	233	1210	0.45	26
LiF-23NdF$_3$	1191	0.20[a]	0	20	0.019	312	1486	0.65	34
LiF-23NdF$_3$	1241	0.21[a]	0	20	0.021	309	902	1.1	49
LiF-23NdF$_3$	1291	0.22[a]	0	20	0.023	338	851	1.3	59
LiF-20NdF$_3$	1241	0.20[c]	0	20	0.021[c]	279	772	1.01	49[b]
LiF-15NdF$_3$	1241	0.15[c]	0	20	0.015[c]	258	900	0.74	49[b]
LiF-10NdF$_3$	1241	0.14[c]	0	20	0.014[c]	265	1026	0.68	49[b]
LiF-5NdF$_3$	1241	0.03[c]	0	20	0.003[c]	235	3439	0.16	49[b]
NaF-23NdF$_3$	1141		0	20		240	1827	0.32	
KF-23NdF$_3$	1141		0	20		243	5338	0.11	

[a]The solubility was obtained from ref 22, and the density of the melt was calculated according to the data from ref 9. [b]Values are taken from that in LiF-23NdF$_3$ at 1241 K. [c]Values are calculated assuming that the diffusion coefficient is independent of composition and is the same as that in LiF-23NdF$_3$ at 1241 K. [d]T is the temperature, and D is the diffusion coefficient.

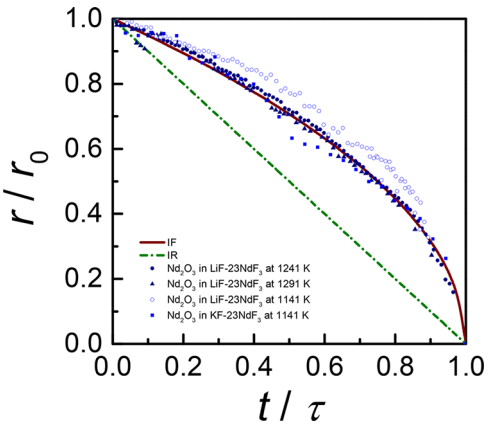

Figure 4. Dissolution curves of Nd_2O_3 particles in fluoride melts.

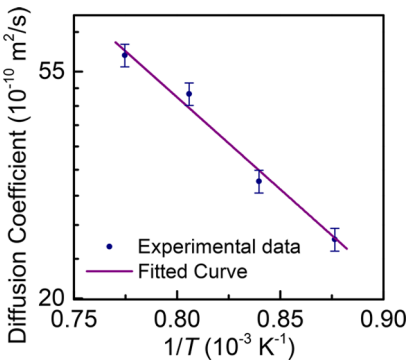

Figure 5. Experimental values (symbols) for the diffusion coefficient of Nd_2O_3 in molten LiF-23NdF$_3$, fitted with eq 10 (solid line).

Some representative data from the CSLM experiments are selected and shown in Figure 4. It shows that the shrinkage of the Nd_2O_3 particle follows the trend of the diffusion-controlled process. This confirms that the dissolution of a Nd_2O_3 particle in molten fluorides is diffusion-controlled, and the IF approximation can be employed to describe the dissolution process.

3.3. Diffusion Coefficient of Nd_2O_3 in LiF-NdF$_3$. The total dissolution time in the case of diffusion control can be calculated by[19]

$$\tau = \frac{r_0^2}{kD} \tag{8}$$

In this paper, the Nd_2O_3-fluoride system is treated as a quasi-binary system of a solute (Nd_2O_3) and a solvent (the binary melt). The diffusion coefficient D represents the effective diffusion of Nd_2O_3 in the melt.

With the experimental data, including the total dissolution time, original particle radius, and k values, it is possible to calculate the diffusion coefficients (see Table 3 and Figure 5). Expectedly, the diffusion coefficients increase with temperature, indicating enhanced diffusion at high temperature. The diffusion coefficient correlates with temperature, following the Arrhenius equation

$$D = D_0 \exp\left(-\frac{E_A}{RT}\right) \tag{9}$$

where D_0 is the pre-exponential factor in m^2/s, R is the universal gas constant, and E_A is the activation energy for diffusion in J/mol. The fit of eq 9 to the experimental data in Figure 5 yields an activation energy of 68 kJ/mol for diffusion and a pre-exponential factor $D_0 = 3.2 \times 10^{-6}$ m^2/s. Thus, in LiF-23NdF$_3$, the diffusion coefficient of Nd_2O_3 can be calculated via

$$D_{Nd_2O_3} = 3.2 \times 10^{-6}\ \text{m}^2/\text{s} \times \exp\left(-\frac{6.8 \times 10^4\ \text{J/mol}}{RT}\right) \tag{10}$$

With the k values and eq 10, it is possible to estimate the total dissolution time of Nd_2O_3 particles in LiF-23NdF$_3$ in the temperature range of 1141−1291 K. These parameters are also essential for the numerical simulations of more complex processes, for instance, the dissolution of feed materials in an industrial electrolytic cell with forced mixing effects introduced by generated CO and CO_2 bubbles at the anodes during electrolysis.

For dilute solutions, the diffusion coefficient is often viewed as a parameter independent of composition. The Nd_2O_3 solubility in LiF-NdF$_3$ is quite low, and it is, therefore, reasonable to assume that the diffusion coefficient remains unchanged in LiF-NdF$_3$ melts with different NdF$_3$ concentrations. To validate this hypothesis, the Nd_2O_3 solubility is calculated, assuming that the diffusion coefficient is independent of salt composition. The results are listed in Table 3 and shown in Figure 6. Assuming a linear relationship of the solubility to NdF$_3$ concentration yields a rather good fitting (R^2 = 0.97). The gap between the second point and the fitted line suggests that this is a bad datum, and the experiment needs repeating. As other data have already demonstrated the

DOI: 10.1021/acs.iecr.7b04125
Ind. Eng. Chem. Res. 2018, 57, 1380−1388

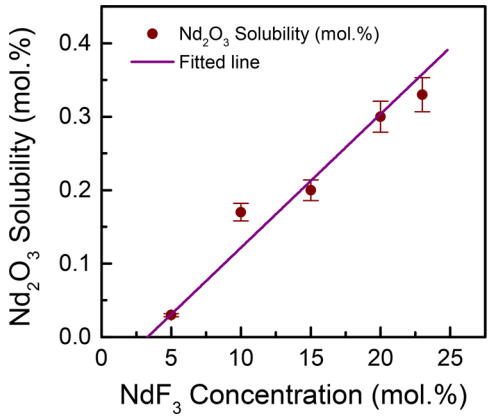

Figure 6. Solubility of Nd_2O_3 in LiF-NdF_3 at 1241 K.

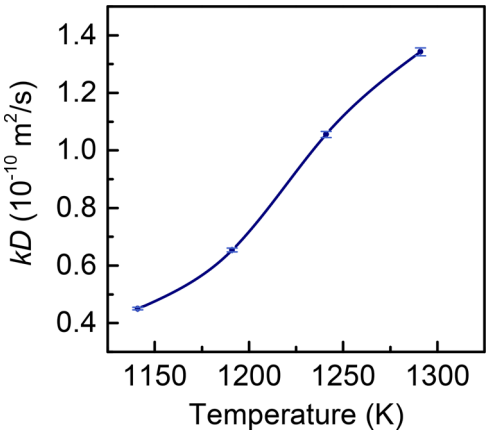

Figure 7. Product *kD*, determining Nd_2O_3 dissolution in LiF-23NdF_3, as a function of temperature.

linearity, the bad datum can be ignored in this paper. This linear relationship agrees well with the conclusion from ref 21, which confirms that a composition-independent diffusion coefficient is a valid assumption. With this conclusion, it is possible to extend the application of the diffusion coefficient obtained previously. This means that eq 10 can be applied to estimate the diffusion coefficient of Nd_2O_3 in LiF-NdF_3 melt with 5−23 mol % NdF_3 at 1141−1291 K.

3.4. Influencing Factors. *3.4.1. Temperature.* According to eq 8, the total dissolution time is inversely proportional to the value of *kD*, suggesting that Nd_2O_3 particles dissolve faster in the melts with higher *kD* values. The factors that influence the diffusion coefficient *D* and supersaturation ratio *k* determine the dissolution rate. In this study, the diffusion coefficient is a function of temperature and is independent of salt composition (eq 10). According to the definition of *k* (eq 2), it is a parameter correlated to the solubility of Nd_2O_3, molar volume, and composition of the melt. The Nd_2O_3 solubility and melt density are functions of temperature and salt composition. Thus, the influence of these factors, i.e., temperature and salt composition, will be discussed based on the experimental observations in the following sections.

The product of *D* and *k* in LiF-23NdF_3 at different temperatures have been derived by means of eq 8 from the observed completion time τ in combination with the initial radius r_0. The results are shown in Figure 7. The *kD* values increase with temperature, suggesting that the dissolution rate is enhanced at elevated temperatures.

The effects of temperature on the diffusion coefficient are given in eq 10. It is evident that the diffusion coefficient increases with temperature. According to the experimental conditions, Nd_2O_3 was not present in the original melts, i.e., $C_M = 0$. The influence on the *k* values merely reflects the change of the solubility and molar volume.

The previous research[22] shows that the relationship between solubility and temperature can be expressed as

$$s_{Nd_2O_3} = x \exp\left(-\frac{A}{RT}\right) \tag{11}$$

where *x* is a function related to the melt composition, and *A* is a positive constant in J/mol. For LiF-NdF_3 melt,[22] the Nd_2O_3 solubility can be calculated via[22]

$$s_{Nd_2O_3}(\text{mol }\%) = (1.1x_{NdF_3} - 0.12x_{LiF}) \exp\left(-\frac{40\text{ kJ/mol}}{RT}\right) \tag{12}$$

where x_i is the mole fraction of compound *i* in the original melt without dissolved Nd_2O_3. It is easy to figure out that the Nd_2O_3 solubility in LiF-NdF_3 increases with temperature.

The melt density has a linear relationship with temperature, expressed as[23]

$$\rho = a - bT \tag{13}$$

where ρ is the melt density in g/cm^3 at temperature *T*, and *a* and *b* are two positive constants. The relationship shown in eq 13 is retained for both pure compounds and mixtures. The values of *a* and *b* depend on melt composition. The molar volume is correlated to the density via

$$V_m = \frac{M}{1000\rho} \tag{14}$$

where *M* is the molecular weight in g/mol. According to eqs 13 and 14, the melt density decreases with temperature, while the molar volume increases with temperature.

The solubility of Nd_2O_3 in fluorides is somewhat limited, usually far less than 1 mol %.[22] Its influence on the molar volume of the salts can be ignored. In this paper, the solution with dissolved Nd_2O_3 will be treated as a quasi-binary salt system for density calculations. Due to the lack of the density data of LiF-NdF_3 melt, its molar volume will be calculated from the density of pure LiF and NdF_3. The molar volume of an ideal binary mixture can be calculated from

$$V_m = x_1V_{m1} + x_2V_{m2} \tag{15}$$

where V_{m1}, V_{m2} are the molar volumes of the respective components. For AF-REF binary systems containing LiF, the real values agree quite well with the estimated values from ideal mixtures.[23] In this paper, all binary salts will be treated as ideal mixtures when calculating their molar volumes.

The values of the parameters in eq 13 are obtained for LiF and NdF_3 from ref 9, see Table 4. These parameters are used for calculating the molar volume of LiF and NdF_3 at different temperatures.

Combining eqs 12−15 and parameters in Table 4, the *k* values in LiF-NdF_3 with different NdF_3 concentrations and at different temperatures are calculated and shown in Figure 8. It is clear that the *k* values increase with temperature in the temperature and composition range concerned.

As shown in Figure 5 and Figure 8, both *k* and *D* in LiF-NdF_3 melt increase with temperature in the temperature range

DOI: 10.1021/acs.iecr.7b04125
Ind. Eng. Chem. Res. 2018, 57, 1380−1388

Table 4. Parameters for Calculating the Density of LiF and NdF_3

	a^a (g/cm^3)	b^a (10^{-3}g/(cm^3·K))
LiF	12	7.5
NdF_3	9.0	2.9

[a]Calculated from data in ref 9.

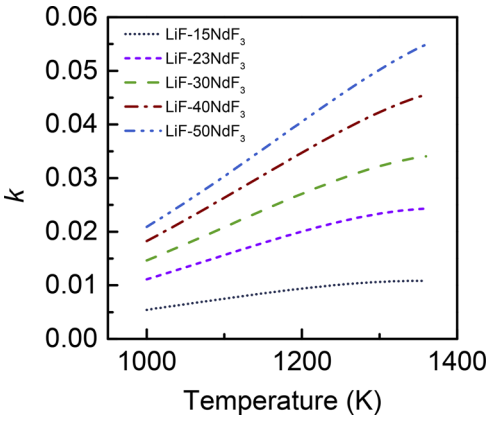

Figure 8. Calculated k values in LiF-NdF_3 with different NdF_3 concentrations and at different temperatures.

of this study. Increasing temperature can accelerate the dissolution of Nd_2O_3 in LiF-NdF_3 melt. With the increase in NdF_3 content, the dependence of k on temperature becomes more significant (Figure 8). This influence extends to the dissolution rate, and the temperature has more impacts on the dissolution rate in the melt with higher NdF_3 content.

3.4.2. NdF_3 Concentration. The dissolution of Nd_2O_3 in LiF-NdF_3 melts with different NdF_3 concentrations was observed, and the results show that increasing NdF_3 concentration can accelerate the dissolution (see Table 3). It can be found that the kD values increase with varying NdF_3 concentration as shown in Figure 9.

As discussed previously, the diffusion coefficient is independent of the salt composition. Therefore, the influence of NdF_3 concentration mainly acts on the k values, more precisely, on the Nd_2O_3 solubility and molar volume of the melt.

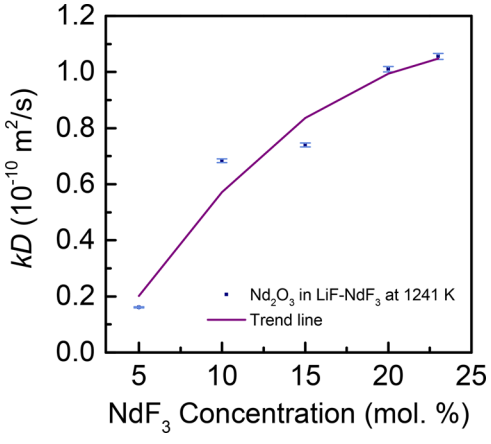

Figure 9. Experimental values of kD as a function of NdF_3 concentration in LiF-NdF_3 at 1241 K (the solid line is a guide to the eye).

According to eqs 11 and 12, the Nd_2O_3 solubility is proportional to the NdF_3 concentration in LiF-NdF_3 melt.[21] Even though eq 12 is not suitable to estimate the solubility in LiF-NdF_3 with a NdF_3 concentration lower than 10 mol %, the proportional relationship between the solubility and NdF_3 concentration is retained.[21] Thus, the solubility can be expressed as

$$s_{Nd_2O_3} = m + nx_{NdF_3} \tag{16}$$

where m and n are constants. Per eq 15, the molar volume of LiF-NdF_3 can be calculated via

$$\begin{aligned} V_{m(LiF-NdF_3)} &= x_{LiF}V_{m(LiF)} + x_{NdF_3}V_{m(NdF_3)} \\ &= V_{m(LiF)} + (V_{m(NdF_3)} - V_{m(LiF)})x_{NdF_3} \end{aligned} \tag{17}$$

where the molar volume of LiF and NdF_3, i.e., $V_{m(LiF)}$ and $V_{m(NdF_3)}$, can be obtained based on the data in Table 4. Therefore, the composition dependence of k can be expressed as

$$\begin{aligned} \frac{\partial k}{\partial x_{NdF_3}} &= \frac{2}{C_P}\cdot\frac{\partial C_I}{\partial x_{NdF_3}} = \frac{2}{C_P}\cdot \\ &\frac{nV_{m(LiF)} - m(V_{m(NdF_3)} - V_{m(LiF)})}{[V_{m(LiF)} + (V_{m(NdF_3)} - V_{m(LiF)})x_{NdF_3}]^2} = c \end{aligned} \tag{18}$$

Thus,

$$\frac{\partial(kD)}{\partial x_{NdF_3}} = D\frac{\partial k}{\partial x_{NdF_3}} = cD \tag{19}$$

The experimental results (Table 3 and Figure 9) show that the value of kD increases with NdF_3 concentration, which indicates that c is positive. In addition, c is a parameter decreasing with increasing NdF_3 concentration, indicating that the gradient of the curve decreases with increasing concentration. The shape of the trend line in Figure 9 is consistent with this conclusion.

3.4.3. Alkali Metal Fluorides. Figure 10 shows the influence of the type of alkali metal fluoride on Nd_2O_3 dissolution in AF-23NdF_3. The dissolution rate decreases in the order from LiF-23NdF_3, NaF-23NdF_3, to KF-23NdF_3. This supports the choice of LiF-NdF_3 as an electrolyte in commercial production concerning the dissolution rate.

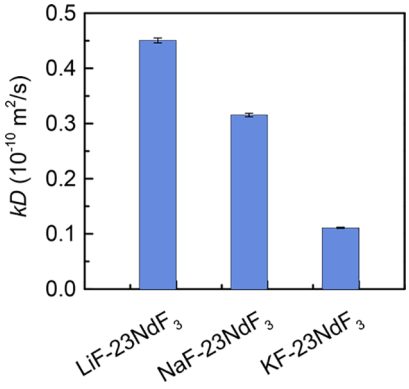

Figure 10. Influence of type of alkali metal fluoride on Nd_2O_3 dissolution in AF-23NdF_3 at 1141 K.

The molar volumes of LiF, NaF, and KF at specific temperature increase in the order of their atomic weight, i.e.,

DOI: 10.1021/acs.iecr.7b04125
Ind. Eng. Chem. Res. 2018, 57, 1380−1388

$V_{m(LiF)} < V_{m(NaF)} < V_{m(KF)}$.[23] According to eq 15, it can be derived that

$$V_{m(LiF\text{-}23NdF_3)} < V_{m(NaF\text{-}23NdF_3)} < V_{m(KF\text{-}23NdF_3)} \quad (20)$$

The solubility of rare earth oxides is found to be associated with the charge density of the cations in the melt.[22] With higher charge density, it is more likely to form stable M−O−F (M = metal) complex anions, which are the products of the interaction between Nd_2O_3 and the fluoride melt.[22] Higher concentration of the M−O−F complex in the Nd_2O_3-fluoride system means that the melt dissolves more Nd_2O_3. The concentration of NdF_3 is the same in these three melts. Given the same Nd^{3+} concentration, it only needs to compare the charge density of the other cation in the melt. As indicated in ref 22, the charge density decreases in the order of Li^+, Na^+, and K^+. It can be inferred that the Nd_2O_3 solubility should decrease in the order of LiF-23NdF_3, NaF-23NdF_3, and KF-23NdF_3, i.e.,

$$s_{LiF\text{-}23NdF_3} > s_{NaF\text{-}23NdF_3} > s_{KF\text{-}23NdF_3} \quad (21)$$

According to eq 4, this implies

$$C_{I(LiF\text{-}23NdF_3)} > C_{I(NaF\text{-}23NdF_3)} > C_{I(KF\text{-}23NdF_3)} \quad (22)$$

As per its definition (eq 6), the parameter k of the systems follows the order

$$k_{LiF\text{-}23NdF_3} > k_{NaF\text{-}23NdF_3} > k_{KF\text{-}23NdF_3} \quad (23)$$

Since absolute k values are not available, it is not possible to obtain the diffusion coefficient in NaF/KF-23NdF_3. Nevertheless, the dissolution experiments in this study confirm that LiF-NdF_3 is a suitable solvent for Nd_2O_3 regarding kinetic aspects. Also, the solubility in LiF-NdF_3 is higher than that in NaF/KF-23NdF_3, which means that the former is a better solvent considering the thermodynamic factor. As an electrolyte, the addition of LiF can improve the electrical conductivity of the melt due to the low resistance of movement and high mobility of Li^+ cation.[9] Considering all these advantages, LiF-NdF_3 is justifiably chosen as the primary electrolyte for electrowinning neodymium in industrial production.

4. CONCLUSIONS

In this research, the dissolution behavior of Nd_2O_3 particles in molten fluorides was investigated via *in situ* observation with CSLM, providing a better understanding of the dissolution mechanisms and its influencing factors, i.e., temperature, salt type, and composition, and offering a method to estimate the dissolution time in LiF-NdF_3 melt. The main conclusions can be formulated as follows:

1) The dissolution of Nd_2O_3 in molten fluoride is a diffusion-controlled process. The diffusion coefficient increases from 2.6 × 10^{-9} to 5.9 × 10^{-9} m^2/s when the temperature rises from 1141 to 1291 K, and the activation energy is determined to be 68 kJ/mol.

2) Increasing temperature and NdF_3 concentration in LiF-NdF_3 melt can accelerate the dissolution, while LiF-23NdF_3 is shown to be a better solvent for Nd_2O_3 than NaF-23NdF_3 and KF-23NdF_3 regarding the dissolution rate.

3) The activation energy for diffusion and the pre-exponential factor D_0 obtained are two critical parameters in this kinetic study. Together with solubility and density data, it is possible to estimate the total dissolution time of Nd_2O_3 in LiF-NdF_3 melt with 5−23 mol % NdF_3 in the temperature range of 1141−1291 K.

AUTHOR INFORMATION

Corresponding Authors

*E-mail: x.guo-1@tudelft.nl (X.G.).
*E-mail: zhisun@126.com (Z.S.).

ORCID

Xiaoling Guo: 0000-0001-6396-6396
Zhi Sun: 0000-0001-7183-0587

Notes

The authors declare no competing financial interest.

ACKNOWLEDGMENTS

The authors appreciate Dr. Abhishek Mukherjee's generous help for the CSLM experiments. The authors would like to acknowledge the EU FP7 project REEcover (Project ID: 603564) for financial support of this study and CAS Pioneer Hundred Talents Program for supporting the work from Dr. Zhi Sun.

REFERENCES

(1) Goonan, T. G. *Rare Earth Elements--End Use and Recyclability*; US Department of the Interior, US Geological Survey: Reston, 2011.

(2) Tanaka, M.; Oki, T.; Koyama, K.; Narita, H.; Oishi, T. Recycling of Rare Earths from Scrap. In *Handbook on the Physics and Chemistry of Rare Earths*; Jean-Claude, G. B., Vitalij, K. P., Eds.; Elsevier: Amsterdam, 2013; Vol. *43*, pp 159−211, DOI: 10.1016/B978-0-444-59536-2.00002-7.

(3) Rollat, A.; Guyonnet, D.; Planchon, M.; Tuduri, J. Prospective Analysis of the Flows of Certain Rare Earths in Europe at the 2020 Horizon. *Waste Manage. (Oxford, U. K.)* **2016**, *49*, 427−436.

(4) (a) Sun, Z.; Cao, H.; Xiao, Y.; Sietsma, J.; Jin, W.; Agterhuis, H.; Yang, Y. Toward Sustainability for Recovery of Critical Metals from Electronic Waste: The Hydrochemistry Processes. *ACS Sustainable Chem. Eng.* **2017**, *5* (1), 21−40. (b) Sun, Z.; Xiao, Y.; Sietsma, J.; Agterhuis, H.; Yang, Y. Recycling of Metals from Urban Mines − a Strategic Evaluation. *J. Cleaner Prod.* **2016**, *112*, 2977−2987.

(5) European Commission *Commission Communication on the 2017 List of Critical Raw Materials for the EU*; European Commission: Brussels, 2017.

(6) Krishnamurthy, N.; Gupta, C. K. *Extractive Metallurgy of Rare Earths*; CRC Press: 2004.

(7) Pang, S.; Yan, S.; Li, Z.; Chen, D.; Xu, L.; Zhao, B. Development on Molten Salt Electrolytic Methods and Technology for Preparing Rare Earth Metals and Alloys in China. *Chin. J. Rare Met.* **2011**, *35* (3), 440−450.

(8) Stefanidaki, E.; Photiadis, G. M.; Kontoyannis, C. G.; Vik, A. F.; Ostvold, T. Oxide Solubility and Raman Spectra of NdF_3-LiF-KF-MgF_2-Nd_2O_3 Melts. *J. Chem. Soc., Dalton Trans.* **2002**, No. 11, 2302−2307.

(9) Hu, X. Study on Ionic Structure and Its Application of NdF_3-LiF-Nd_2O_3 System Melts. Ph.D. Dissertation, Northeastern University, Shenyang, 2008.

(10) Mukherjee, A.; Dyck, J.; Blanpain, B.; Guo, M. CSLM Study on the Interaction of Nd_2O_3 with $CaCl_2$ and CaF_2-LiF Molten Melts. *J. Mater. Sci.* **2017**, *52* (3), 1717−1726.

(11) Perry, D. L. *Handbook of Inorganic Compounds*; 2nd ed.; CRC Press, Taylor & Francis Group: Boca Raton, FL, 2011.

(12) Inaba, H. Semi-Empirical Estimation of Thermal Expansion Coefficients of Oxides. *Jpn. J. Appl. Phys.* **1996**, *35* (Part 1, No. 9A), 4730.

(13) Sun, Z. H. I.; Guo, X.; Van Dyck, J.; Guo, M.; Blanpain, B. Phase Evolution and Nature of Oxide Dissolution in Metallurgical Slags. *AIChE J.* **2013**, *59* (8), 2907−2916.

(14) Brown, L. C. Shape Changes During Dissolution of Theta-$CuAl_2$. *Metall. Trans. A* **1984**, *15* (3), 449−458.

(15) Cooper, A. R.; Kingery, W. D. Dissolution in Ceramic Systems: I, Molecular Diffusion, Natural Convection, and Forced Convection

DOI: 10.1021/acs.iecr.7b04125
Ind. Eng. Chem. Res. 2018, 57, 1380−1388

Studies of Sapphire Dissolution in Calcium Aluminum Silicate. *J. Am. Ceram. Soc.* **1964**, *47* (1), 37−43.
(16) (a) Liu, J.; Verhaeghe, F.; Guo, M.; Blanpain, B.; Wollants, P. In Situ Observation of the Dissolution of Spherical Alumina Particles in $CaO-Al_2O_3-SiO_2$ Melts. *J. Am. Ceram. Soc.* **2007**, *90* (12), 3818−3824. (b) Verhaeghe, F.; Liu, J.; Guo, M.; Arnout, S.; Blanpain, B.; Wollants, P. Dissolution and Diffusion Behavior of Al_2O_3 in a $CaO-Al_2O_3-SiO_2$ Liquid: An Experimental-Numerical Approach. *Appl. Phys. Lett.* **2007**, *91* (12), 124104. (c) Feichtinger, S.; Michelic, S. K.; Kang, Y. B.; Bernhard, C. In Situ Observation of the Dissolution of SiO_2 Particles in $CaO-Al_2O_3-SiO_2$ Slags and Mathematical Analysis of Its Dissolution Pattern. *J. Am. Ceram. Soc.* **2014**, *97* (1), 316−325.
(17) Aaron, H.; Kotler, G. Second Phase Dissolution. *Metall. Trans. A* **1971**, *2* (2), 393−408.
(18) Levenspiel, O. *Chemical Reaction Engineering*, 3rd ed.; John Wiley & Sons: New York, 1999.
(19) Aaron, H. B.; Fainstein, D.; Kotler, G. R. Diffusion-Limited Phase Transformations - a Comparison and Critical Evaluation of Mathematical Approximations. *J. Appl. Phys.* **1970**, *41* (11), 4404−4410.
(20) Guo, X.; Sietsma, J.; Yang, Y.; Sun, Z.; Guo, M. Diffusion-Limited Dissolution of Spherical Particles: A Critical Evaluation and Applications of Approximate Solutions. *AIChE J.* **2017**, *63* (7), 2926−2934.
(21) Guo, X.; Sietsma, J.; Yang, Y. A Critical Evaluation of Solubility of Rare Earth Oxides in Molten Fluorides. In *Rare Earths Industry*; de Lima, I. B., Filho, W. L., Eds.; Elsevier: Boston, 2016; pp 223−234, DOI: 10.1016/B978-0-12-802328-0.00015-2.
(22) Guo, X.; Sun, Z.; Sietsma, J.; Yang, Y. Semiempirical Model for the Solubility of Rare Earth Oxides in Molten Fluorides. *Ind. Eng. Chem. Res.* **2016**, *55* (16), 4773−4781.
(23) Porter, B.; Meaker, R. E. *Density and Molar Volumes of Binary Fluoride Mixtures*; Department of the Interior, Bureau of Mines: WA, 1966.

DOI: 10.1021/acs.iecr.7b04125
Ind. Eng. Chem. Res. 2018, 57, 1380−1388